ISSN 1054-660X, Laser Physics, 2010, Vol. 20, No. 3, pp. 709–715.

Generation of High-Energy Pulses from an All-Normal-Dispersion Figure-8 Fiber Laser[1]

O. Pottiez[a, *], B. Ibarra-Escamilla[b], E. A. Kuzin[b], R. Grajales-Coutiño[a], C.-M. Carrillo-Delgado[a]

[a] *Centro de Investigaciones en Óptica (CIO), Loma del Bosque 115, Col. Lomas del Campestre, León, Gto. 37150, Mexico*

[b] *Instituto Nacional de Astrofísica, Óptica y Electrónica (INAOE), Departamento de Óptica, L. E. Erro 1, Puebla, Pue. 72000, Mexico*

*e-mail: pottiez@cio.mx

Received August 6, 2009; in final form September 24, 2009; published online February 2, 2010

Abstract—We propose and study numerically an all-normal-dispersion Ytterbium-doped figure-eight fiber laser scheme for generation of high-energy pulses. The monotonous pulse stretching that takes place in the fiber under the combined actions of normal dispersion and nonlinear Kerr effect is compensated by the amplitude modulation effect of a bandpass filter inserted in the ring section of the laser. The Nonlinear Optical Loop Mirror (NOLM) also contributes to shorten the pulses. An output coupler with a large output coupling ratio is inserted at the amplifier output in order to extract the maximal energy from the laser. A short segment of Ytterbium-doped fiber compensates for the losses. Stable single-pulse operation is predicted over a wide range of values of the laser parameters. If the laser parameters (ring and NOLM length, dispersion, filter bandwidth, output coupling ratio) are optimized, pulses with several tens of nanojoules energy are readily obtained, with picosecond duration and a large positive chirp which is linear near the peak. If small-signal gain is large enough, the use of very large output coupling ratios opens the way to pulse energies close to 100 nJ and, after dechirping outside the laser, to durations of ~50 fs and peak powers of 1 MW.

DOI: 10.1134/S1054660X10050166

1. INTRODUCTION

In spite of their high efficiency and waveguide nature, which makes them insensitive to alignment problems, mode-locked fiber lasers are often discarded at the benefit of solid-state lasers for applications requiring high pulse energies. Their limitation in pulse energy and peak power results from the intrinsic nonlinearity of the fiber, where light is tightly confined into the core and where the nonlinear phase shift accumulates over relatively long distances, ultimately provoking pulse breaking. In anomalous-dispersion soliton fiber lasers, where pulse formation results from a balance between Kerr nonlinearity and anomalous dispersion, pulse energy is limited to ~0.1 nJ [1]. By using the concept of dispersion management as a strategy to reduce effective peak power, this limit was increased to 2–3 nJ with the so-called stretched-pulse fiber lasers [2, 3]. Pulse energies higher than 10 nJ were recently obtained from a mode-locked fiber laser in the anomalous-dispersion regime, however the use of large-mode-area photonic crystal fiber was required [4].

Many research activities today focus on ytterbium-doped fibers, in particular for the design high-power laser sources [5–10]. In the frame of ultrashort-pulse generation however, fiber lasers emitting in the 1 μm region do not allow in general conventional mode locking, as the fiber dispersion is normal at this wavelength. It was recently demonstrated however that very high pulse energies can be obtained with lasers operating at 1 μm in the normal dispersion regime [11]. In this regime, the pulse tends to develop a positive linear chirp under the combined effects of nonlinear phase shift and normal dispersion. A bandpass filter stabilizes the intracavity evolution by removing the wavelength-shifted edges at each cycle. A saturable absorber (SA) mechanism is also needed to ensure pulsed operation. The duration of the generated pulses is several times the transform limit, and dechirping is performed outside the laser by the use of the appropriate amount of anomalous dispersion. After this operation, high-energy, high-peak-power, nearly transform-limited pulses with ~100 fs duration are obtained. Pulse energies above 10 nJ and peak powers close to ~100 kW were obtained in this regime [12, 13].

In most of these works in the normal dispersion regime, the passively mode-locked laser architectures were ring cavities, in which the effective SA mechanism is provided by nonlinear polarization rotation (NPR) in the ring together with a polarizer (exceptions can be found in [14, 15]). Although most of these schemes are Ytterbium-doped fiber lasers operating at 1 μm, where the standard fiber exhibits normal dispersion, they also include an anomalous dispersion segment for dispersion compensation, which usually takes the form of a bulk grating pair. As a consequence,

[1] The article is published in the original.

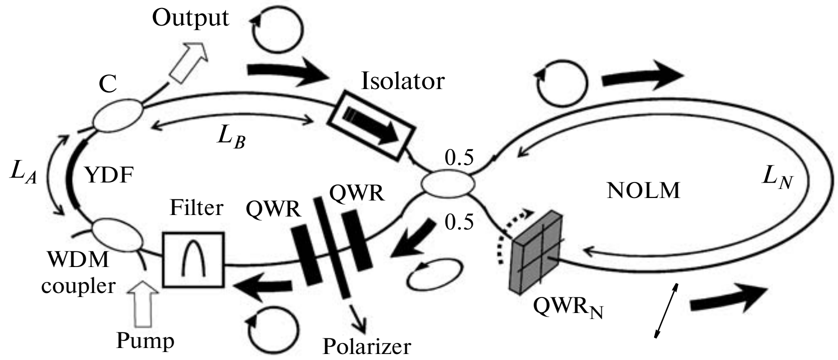

Fig. 1. Scheme of the laser under study. YDF: Ytterbium-doped fiber.

the resulting setup is not all-fiber and loses the benefits of the waveguide medium. Another noteworthy result is the generation of pulses with energies as high as 75 nJ by using a very long linear cavity and a semiconductor saturable absorber mirror (SESAM) [15]. Again, the benefits of the all-fiber configuration are lost through the use of a semiconductor element. In [16, 17] however, all-normal-dispersion ring lasers were demonstrated experimentally. In spite of the very large amount of normal intracavity dispersion in comparison with the dispersion compensated schemes, stable pulsed operation was reported, although pulse energies were not larger than a few nanojoules.

The possibility to operate a figure-eight fiber laser in the normal dispersion regime was first demonstrated experimentally in [14], although moderate pulse energies (1.5 nJ) were reported. In this paper we demonstrate numerically that stable high-energy pulses can be generated using an all-normal-dispersion figure-eight fiber laser. In this scheme, the saturable absorber action is due to a Nonlinear Optical Loop Mirror (NOLM) [18]. In contrast to the ring configuration, the figure-eight architecture avoids pulse energy limitation due to overdriving the saturable absorber, as switching does not rely on the accumulation of nonlinear phase shift over the whole cavity but only in the NOLM, whose length can be easily shortened [11, 19]. We analyze pulse evolution in the cavity and study how the laser parameters (including fiber dispersion, NOLM length and low-power transmission, output coupling ratio and filter bandwidth) affect the energy of the pulses that are obtainable.

2. MODEL

The figure-eight laser scheme under study is shown in Fig. 1. The NOLM is a power-symmetric structure whose operation relies on NPR instead of self-phase modulation (SPM) [20]. It includes a symmetrical coupler, a section of circularly birefringent (twisted) fiber, and a quarter-wave retarder (QWR_N) located asymmetrically in the loop. The QWR_N ensures that the counter-propagating beams have different polarizations and accumulate different amounts of NPR, thus allowing switching. The fiber loop has a length L_N. The input polarization to the NOLM is circular, say right, and the orthogonal (left) circular polarization is selected at its output, through the use of a QWR and a polarizer. The combination NOLM + QWR + polarizer presents a sinusoidal nonlinear transfer characteristic, whose minimum and maximum values are 0 and 0.5, respectively, and whose low-power transmission can be adjusted precisely through the QWR_N orientation [21, 22]. Another QWR following the polarizer converts linear polarization back to circular right. This polarization state is assumed to be maintained to the NOLM input. The ring includes a Gaussian bandpass filter with full width at half maximum (FWHM) bandwidth $\Delta\lambda$, and a short length L_A of Ytterbium-doped fiber characterized by its small-signal gain per unit length and saturation energy. An additional section L_B of fiber is inserted at the NOLM input. All fiber segments in the cavity, including the NOLM loop, doped fiber and the L_B section are assumed to present the same normal dispersion D (or β_2) and nonlinear coefficient (for circular polarization) $\gamma_c = 5$ W/km. An optical isolator and an output coupler with coupling ratio C:$1 - C$, thus introducing a loss $1/(1 - C)$ complete the cavity. The location of the coupler at the amplifier output is intended to extract the maximal energy from the laser.

The laser operation is studied through numerical simulations. Propagation in the fiber sections is modeled using a pair of extended nonlinear Schrödinger equations, which are integrated using the Split-Step Fourier (SSF) method. In the circular polarization basis $[C^+, C^-]$, the general form of these equations is [23]

$$\begin{aligned}\frac{\partial C^+}{\partial z} &= -j\frac{\beta_2}{2}\frac{\partial^2 C^+}{\partial t^2} + j\gamma_c(|C^+|^2 + 2|C^-|^2)C^+ + \frac{g}{2}C^+,\\ \frac{\partial C^-}{\partial z} &= -j\frac{\beta_2}{2}\frac{\partial^2 C^-}{\partial t^2} + j\gamma_c(|C^-|^2 + 2|C^+|^2)C^- + \frac{g}{2}C^-,\end{aligned} \quad (1)$$

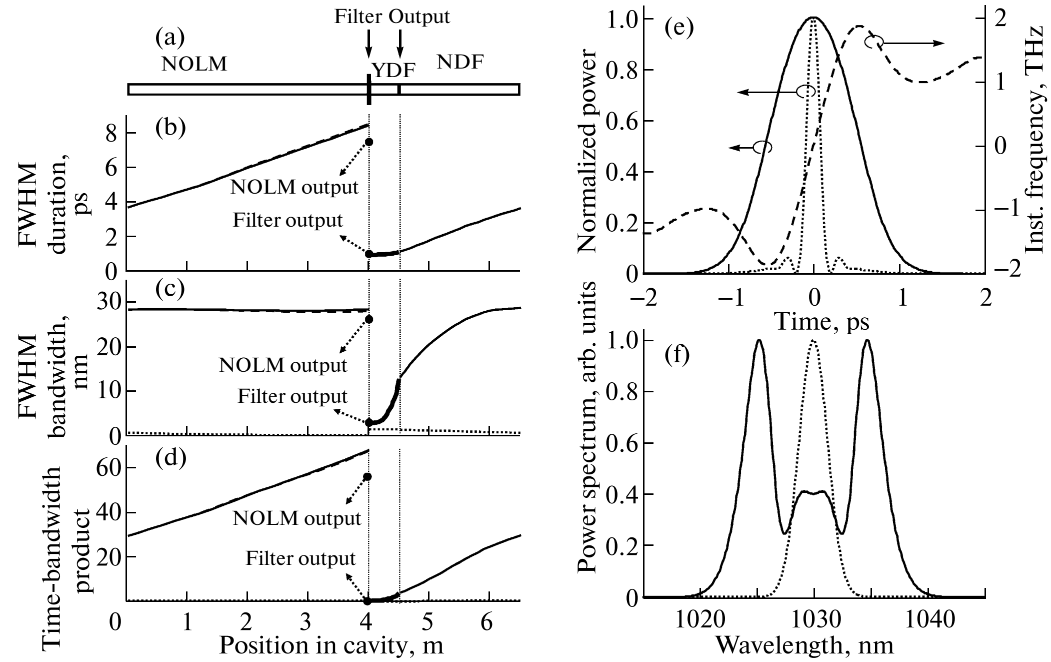

Fig. 2. (a) Schematic diagram of the laser; (b) FWHM pulse duration, (c) bandwidth and (d) time-bandwidth product of the pulse along the cavity. Inside the NOLM, solid and dashed lines correspond to CW and CCW beams, respectively; dotted lines show the bandwidth and time-bandwidth product of the transform-limited pulse having the same temporal profile as the actual pulse; values at the NOLM output and at the filter output are indicated by arrows; (e) normalized pulse power profile at the laser output (solid) together with instantaneous frequency (dashed), and normalized power profile of the dechirped pulse (dotted); (f) output pulse spectrum (solid) and filter transmission spectrum (dotted). FWHM filter bandwidth $\Delta\lambda = 2.94$ nm. Other laser parameters are: $L_A = 0.5$ m, $L_B = 2$ m, $L_N = 4$ m, $D = -40$ ps/nm/km, $g_0L_A = 5000$, $E_{sat} = 0.16$ nJ, $\gamma_c = 5$ W/km and low-power NOLM transmission is 7×10^{-4}. YDF: Ytterbium-doped fiber. NDF: normal-dispersion fiber.

where C^+ and C^- are the circular right and left polarization components, respectively. The first two right-hand terms of Eq. (1) are dispersive and Kerr nonlinear terms. The third terms are gain terms, which are considered only for integration over the gain section. The coefficient g is the gain per unit length. Here, g is assumed to be constant across the doped fiber, and saturates on the pulse energy E_p as

$$g(E_p) = \frac{g_0}{1 + E_p/E_{sat}}, \qquad (2)$$

where g_0 is the small-signal gain and E_{sat} is the saturation energy. The spectral dependence of gain is not considered, as its bandwidth is assumed to be larger than the filter bandwidth $\Delta\lambda$. Finally, the twist-induced group-velocity mismatch between circular polarization components, as well as higher-order effects like the Raman self-frequency shift and third-order dispersion were not accounted for, a valid approximation in the normal-dispersion regime, where wide pulses having durations of several picoseconds are formed.

For each set of laser parameters, a small-amplitude Gaussian noise is chosen as the initial signal. More specifically, we choose at the filter input a circular-right polarized signal whose electric field temporal profile is modeled as a Gaussian distribution with zero average and a variance of 1 W. Over each fiber segment, integration is performed using as initial conditions the electric field profile at the output of the preceding section. This signal is propagated over several cycles, and we observe whether a steady-state can be reached or not after a finite number of integration cycles.

3. RESULTS AND DISCUSSION

Stable high-energy pulses presenting large chirp were produced for different sets of laser parameters. Figure 2 shows an unfolded representation of the laser (Fig. 2a) and the evolution of FWHM pulse duration (Fig. 2b), spectral width (Fig. 2c) and time-bandwidth product (Fig. 2d) along the laser in regime, as well as the output pulse profile (Fig. 2e) and spectrum (Fig. 2f), for a particular set of values of the laser parameters. The value $D = -40$ ps/nm/km of dispersion that is chosen for the simulation is typical of standard single-mode fiber around 1 μm.

As expected, the pulse temporal profile expands monotonically through all sections of fiber (Fig. 2b), due to the combined effects of normal dispersion and Kerr nonlinearity. This widening is balanced at each round-trip by the filter and, to a lesser extent, by the

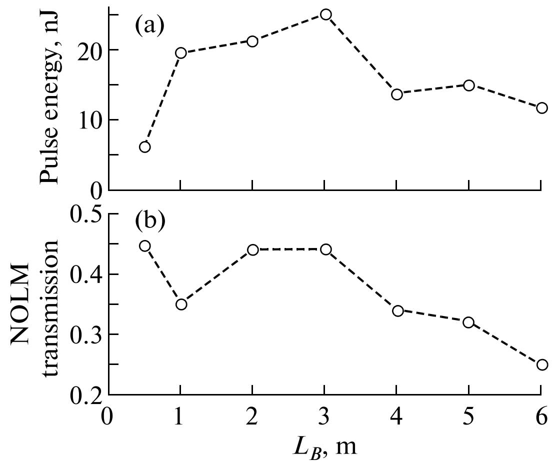

Fig. 3. (a) Maximal output pulse energy and (b) NOLM energy transmission for different values of L_B and maximal E_{sat} allowing single pulse operation. All other laser parameters identical to Fig. 2.

NOLM, which both contribute to reduce the pulse duration. At the filter output, the pulse is nearly transform-limited (Figs. 2c, 2d), however the pulse energy at this point is very low. Indeed, the spectrum of the pulse entering the filter is much wider than the filter bandwidth [dotted line in Fig. 2f], and the energy transmission through the filter is as low as 0.11 in regime. In contrast, the NOLM transmission is 0.42, close to the theoretical maximum value of 0.5. The losses suffered by the pulse due to the filter, NOLM and output coupler are compensated by the saturated gain at each round-trip. The location of the output coupler at the amplifier output allows extracting the highest pulse energy, although chirp is quite large at this point. Using a 80/20 coupler (which extracts 80% of the energy out of the laser), the output pulse energy reaches 11.4 nJ. Figure 2e shows that the pulse is chirped, however its duration of 1.1 ps indicates that chirp at this point is substantially smaller than after propagation through the L_B section, or at the NOLM output. As instantaneous frequency is linear near the peak, the pulse can be compressed down to ~175 fs outside the laser by using an anomalous dispersion of 0.07 ps/nm, a value substantially smaller than the absolute value of the total cavity anomalous dispersion, which is –0.26 ps/nm [dotted line in Fig. 2e]. This duration corresponds to a compression by a factor of 6.4. The pulse is then nearly transform-limited and its peak power reaches more than 50 kW. The output spectrum presents sharp peaks near its steep edges, a feature already observed with the ring laser configuration in the all-normal dispersion regime [16].

Figure 2c shows that the filter strongly reduces the pulse spectral width, which then increases rapidly in the amplifier and L_B sections, where peak power and thus Kerr nonlinearity is high. At the end of the L_B section, however, the spectral width tends to stabilize, as monotonous temporal pulse widening gradually lowers the peak power, thus reducing the magnitude of Kerr nonlinearity. After the 3-dB splitting through the coupler, the bandwidths of the counter-propagating pulses remain practically constant, while their durations continue to increase monotonically through the NOLM loop. In the case presented in Fig. 2, the Kerr effect remains sufficient however to generate a ~π nonlinear phase shift difference between the counter-propagating pulses when they recombine at the coupler, which yields nearly maximal NOLM transmission. This nonlinear phase shift difference depends on the peak power at the NOLM input, which in turn depends on the length $L_A + L_B$. With the parameters of Fig. 2, the pulse peak power at the NOLM input is ~800 W, a value higher than the NOLM switching power calculated for the continuous-wave regime, $P_\pi = 4\pi/\gamma_c L_N = 630$ W, this difference being due to the temporal widening of the pulse taking place in the NOLM, which reduces the effective peak power. Leaving L_A constant, it appears reasonable that, if L_B is increased or decreased with respect to the case of Fig. 2, the peak power at the NOLM input will be decreased or increased, respectively, yielding a nonlinear phase shift difference smaller or higher than π, causing in both cases non-optimal NOLM switching.

Figure 3a presents the dependence of the maximal output pulse energy on the length L_B. In order to estimate the maximum output energy, for each value of L_N, we increased the amplifier saturation energy (which in practice amounts to increasing pump power), until reaching the limit above which a stable single pulse solution is no longer obtained. Figure 3b presents the NOLM energy transmission in each case. For small values of L_B, the pulse output energy is limited by NOLM overdriving. In this case, optimal switching (with NOLM transmission values close to the maximum 0.5) is already reached for moderate values of energy. If energy is further increased, the laser tends to operate in multiple pulsed mode. For large values of L_B, the pulse is highly stretched when it enters the NOLM, and as energy is increased the large nonlinear phase shift in the L_A and L_B sections tends to destabilize the pulse before NOLM switching is reached. Values of NOLM transmission are thus low in this case. The highest pulse energy is observed in Figure 3 for an intermediate value of $L_B = 3$ m. After dechirping outside the laser, the shortest pulses were obtained for $L_B = 1$ to 3 m, with FWHM durations of ~120 fs, corresponding to peak powers of ~140 kW.

We also analyzed the laser operation in function of the NOLM length. Figures 4a and 4b present the dependence of maximal output pulse energy and NOLM transmission on the NOLM length, respectively. For each value of L_N, E_{sat} was raised up to the limit of stable single pulse operation in order to estimate the maximum output energy. For small values of L_N, the NOLM switching power is high, and pulse

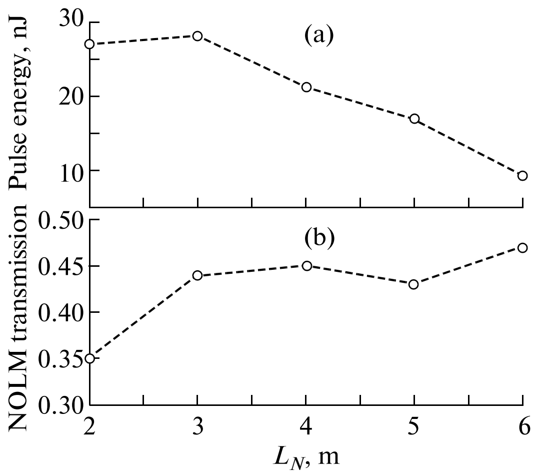

Fig. 4. (a) Maximal output pulse energy and (b) corresponding NOLM transmission for different values of L_N. E_{sat} is set in each case to the maximal value allowing single pulse operation, all other laser parameters are those of Fig. 2.

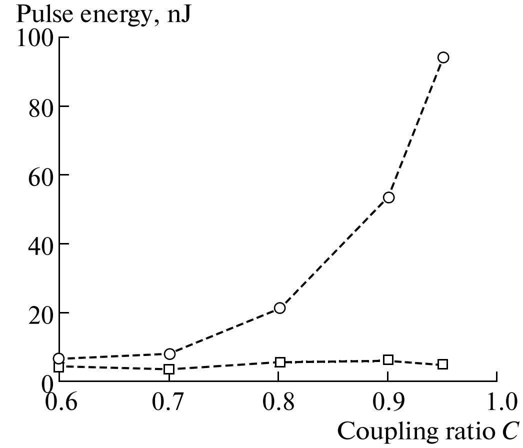

Fig. 5. Maximal output pulse energy (circles) and energy at the complementary output coupler port (squares) for different values of C. E_{sat} is in each case the maximal value allowing single pulse operation, all other laser parameters are those of Fig. 2.

energy is limited by the nonlinear phase shift, which tends to destabilize the pulse before NOLM switching is reached (NOLM transmission is low in this case). In spite of this, large values of pulse energy are obtained in this case. For large values of L_N, the NOLM switching power is low and pulse energy is limited to substantially smaller values, as NOLM overdriving leads to multiple pulse operation. After dechirping, the shortest pulse durations of ~70–80 fs were obtained for $L_N = 2$–3 m, for which the highest pulse energies are also found, yielding peak powers of ~250 kW.

The most spectacular changes in pulse energy are observed when the output coupler coupling ratio is modified. Figure 5 presents the maximal output pulse energy for different values of the coupling ratio. Other laser parameters are kept constant, except the saturation energy which is the highest value that still ensures convergence to a stable single-pulse solution. In general, as could be expected, the output pulse energy is smaller when the output coupling ratio C is smaller. The first obvious reason for this is that a smaller fraction of the energy at the amplifier output is extracted from the amplifier output. The second reason is that, for small values of C, a large fraction $1 - C$ of the pulse energy is re-injected in the laser, so that nonlinear phase shift is strong in the L_B and NOLM sections. The nonlinearity then tends to destabilize the pulse, and ultimately limits the saturation energy for which stable solutions are observed. In contrast, for large values of C, a large fraction of the pulse energy is extracted, and the small value of pulse energy that is re-injected in the laser allows stable single-pulse operation for higher values of saturation energy, before the effects of nonlinearity become too strong. For these reasons, the maximal output energy varies considerably with the coupling ratio, with higher values being obtained for large values of C. In contrast, the energy at the other coupler output port that is injected into the L_B section is nearly constant in all cases (~5 nJ, see Fig. 5). For $C = 0.95$, a pulse whose energy is close to 100 nJ is extracted from the laser. The shortest pulse is also observed in this case after dechirping, with a FWHM duration of only 50 fs, yielding a peak power as high as 1.2 MW. Dechirping requires an amount of anomalous dispersion of 0.02 ps/nm only (much smaller in modules than the –0.26 ps/nm normal dispersion of the cavity), and corresponds to a pulse compression factor of ~26. The insertion loss of the coupler ultimately limits the output pulse energy. Indeed if $C > 0.95$, the low-power cavity losses (due to both coupler and NOLM) are higher than low-power gain, so that lasing can not initiate.

The maximum achievable pulse energy is also influenced by fiber dispersion. Figure 6a presents the maximal pulse energy for which stable solutions were obtained when the saturation energy was increased, for different values of the fiber dispersion. Figure 6b presents in each case the pulse stretching ratio, defined as the ratio between the largest and shortest values taken by the pulse duration in the cavity (prior to recombination at the NOLM output and at the filter output, respectively). Higher pulse energies are attainable for higher values of dispersion, as higher dispersion yields faster temporal widening of the pulse (higher stretching ratio). The pulse can then support higher energies before instabilities due to the nonlinear phase shift can build up, or before NOLM overdriving takes place. The higher pulse energies also correspond to the shorter pulses after dechirping, with 70 to 90 fs FWHM durations and ~250 kW peak power for D from –30 to –50 ps/nm/km.

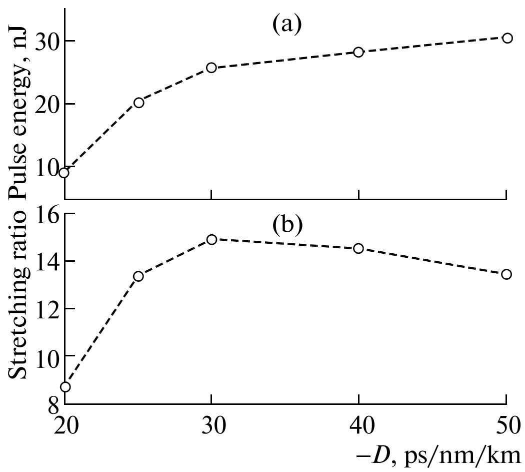

Fig. 6. (a) Maximal output pulse energy and (b) pulse stretching ratio for different values of fibre dispersion D. E_{sat} is in each case the maximal value allowing single pulse operation, and L_N = 3m, all other laser parameters are those of Fig. 2.

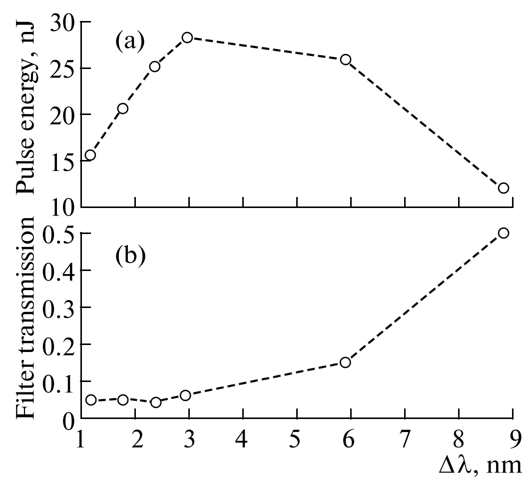

Fig. 7. (a) Maximal output pulse energy and (b) filter energy transmission for different values of FWHM filter bandwidth $\Delta\lambda$. E_{sat} is in each case the maximal value allowing single pulse operation, and L_N = 3 m, all other laser parameters are those of Fig. 2.

Another key parameter that affects the maximal pulse energy is the filter bandwidth. Figure 7a presents maximal pulse energy obtained for different values of the filter bandwidth. Contrary to the results obtained in the case of all-normal-dispersion ring lasers [16], small values of spectral width did not impede convergence, even if a substantial reduction of pulse energy was observed below $\Delta\lambda = 3$ nm. For narrow filter bandwidths, the energy seems to be limited by the filter transmission, which diminishes with increasing power. Indeed, higher pulse energy means higher nonlinear spectral broadening in the fiber, and thus lower transmission through the filter. Filter transmission is as small as ~0.04–0.06 for $\Delta\lambda = 3$ nm and below, which still ensures that small-signal gain be higher than cavity losses. As the filter bandwidth is increased, its transmission increases (Fig. 7b), so that the pulse shortening effect of the filter is gradually reduced. In regime, this means that the pulse stretching that can take place through the fiber sections is reduced, and thus the maximal pulse energy is reduced, too (because the nonlinear phase shift broadens the pulse spectrum, higher energy means broader spectrum and thus stronger pulse stretching in the dispersive fiber). For large values of the spectral width, the filter action is no longer able to compensate for the pulse stretching that takes place in the fiber sections of the cavity, and the pulsed operation is compromised. Taking for example $\Delta\lambda = 12$ nm, good convergence is not observed: a single pulse tends to form, however its energy presents large fluctuations for successive round-trips. The largest pulse energy is obtained for $\Delta\lambda = 3$ nm, and also yields after dechirping the shortest pulse duration of ~80 fs. These values correspond to ~250 kW peak power after dechirping at the laser output.

Finally, we analyzed the effect of the adjustment of the NOLM low-power transmission on the laser operation. Through the QWR_N orientation, the phase of the NOLM transfer characteristic, and thus the low-power transmission can be adjusted between 0 and 0.5. If low-power transmission is too low, the optical power can not build up from initial noise in the cavity because small-signal loss exceeds small-signal gain. With the parameters of Fig. 2, the minimal NOLM low-power transmission still allowing signal buildup is ~10^{-3}, a value consistent with the small-signal gain is 5000 and the output coupler loss is 5. If the low-power NOLM transmission exceeds this value and if the sign of the QWR_N angle ensures a monotonic growth of transmission with power, then stable pulses can be formed. If low-power transmission is increased above ~0.03, however, single-pulse operation is lost. Hence the range of the NOLM low-power transmission over which stable single-pulse operation is found (0.001–0.030) appears to be very narrow in comparison with maximal NOLM transmission (0.5). Such a narrow range corresponds to values of the QWR_N angle extending over a few percents of π, showing that precise adjustment of this parameter is required in practice.

4. CONCLUSIONS

In conclusion, we performed a numerical study of an Ytterbium-doped figure-eight fiber laser designed for the generation of high-energy pulses. The device includes exclusively sections of normally dispersive fiber and operates in the large normal dispersion regime. The monotonous pulse stretching that takes place in the fiber sections of the cavity is balanced by the amplitude modulation of a bandpass filter, assisted by the saturable action of the NOLM. The output coupler presents a large output coupling ratio and is inserted at the amplifier output in order to extract the maximal pulse energy. We showed that stable single-pulse operation is observed over a wide range of variation of the cavity parameters. The maximal output energies are obtained if parameters like the fiber length in the ring, the NOLM length and the fiber dispersion are optimized in order to avoid both NOLM overdriving and pulse breaking induced by excessive nonlinear phase shift. The low-power transmission of the NOLM should also be sufficiently small for convergence to be observed. Finally, large pulse energies are obtained if the filter bandwidth is sufficiently narrow to ensure substantial pulse shortening, although still wide enough to avoid excessive losses at the filter that could not be compensated by gain. For properly optimized parameters, pulse energies of several tens of nanojoules are routinely achieved. After dechirping outside the laser, which can be done by using an amount of anomalous dispersion which is much smaller in modules than the total cavity dispersion, pulses with duration of ~100 fs and a few hundreds of kilowatts peak power are predicted. The pulses presenting higher energies also correspond to shorter values of pulse duration after dechirping. For very high values of the output coupler coupling ratio, even higher pulse energies are theoretically possible, almost reaching 100 nJ. After dechirping outside the laser, nearly transform-limited pulses as short as ~50 fs are predicted, with peak powers that reach the barrier of 1 MW. Such large values of energy and peak power are possible thanks to the short length of Ytterbium-doped fiber that is used, as well as to the position and large coupling ratio of the coupler, ensuring that excessive peak powers do not occur over long segments of fiber in the cavity, thus preventing the development of nonlinear-phase-shift induced pulse breaking. However, as such large coupling ratios correspond to large values of the coupler insertion loss, and because convergence also requires very small values of the NOLM low-power transmission, the total low-power cavity loss is large and must be compensated by the small-signal gain to allow signal buildup in the cavity. The maximum achievable pulse energy thus appears to be limited principally by the value of small-signal gain, as well as the available pump power which determines the saturation energy of the amplifier. The present work shows that all-normal-dispersion Ytterbium-doped figure-eight fiber lasers have the potential to challenge solid-state lasers in the frame of the generation of high-energy ultrashort pulses.

ACKNOWLEDGMENTS

O. Pottiez was supported by CONCYTEG grant 08-04-K662-120 and by CONACyT grant 53990.

REFERENCES

1. I. N. Duling III, Electron. Lett. **27**, 544 (1991).
2. K. Tamura, E. P. Ippen, H. A. Haus, and L. E. Nelson, Opt. Lett. **18**, 1080 (1993).
3. L. E. Nelson, S. B. Fleischer, G. Lenz, and E. P. Ippen, Opt. Lett. **21**, 1759 (1996).
4. B.-W. Liu, M.-L. Hu, X.-H. Fang, Y.-Z. Wu, Y.-J. Song, L. Chai, C.-Y. Wang, and A. M. Zheltikov, Laser Phys. Lett. **6**, 44 (2009).
5. P. Peterka, J. Maria, B. Dussardier. R. Slavik. P. Honzatko, and V. Kubecek, Laser Phys. Lett. **6**, 732 (2009).
6. Q. H. Mao, J. Jiang, X. O. Li, J. H. Chang, and W. O. Liu, Laser Phys. Lett. **6**, 647 (2009).
7. M. R. A. Moghaddam, S. W. Harun, M. R. Tamiis, and H. Ahmad, Laser Phys. Lett. **6**, 586 (2009).
8. S. W. Harun, M. R. A. Moghaddam, K. Dimvati, and H. Ahmad, Laser Phys. Lett. **6**, 458 (2009).
9. P. P. Jiang, D. Z. Yang, Y. X. Wang, T. Chen, B. Wu, and Y. H. Shen, Laser Phys. Lett. **6**, 384 (2009).
10. A. V. Kir'yanov, Yu. O. Barmenkov, F. Mendoza-Santoyo, J. L. Cruz, and M. V. Andres, Laser Phvs. Lett. **5**, 898 (2008).
11. F. O. Ilday, J. R. Buckley, W. G. Clark, and F. W. Wise, Phys. Rev. Lett. **92**, 213902 (2004).
12. J. R. Buckley, F. W. Wise, F. Ö. Ilday, and T. Sosnowski, Opt. Lett. **30**, 1888 (2005).
13. F. O. Ilday, J. R. Buckley, H. Lim, F. W. Wise, and W. G. Clark, Opt. Lett. **28**, 1365 (2003).
14. J. W. Nicholson, S. Ramachandran, and S. Ghalmi, Opt. Express **15**, 6623 (2007).
15. M. Zhang, L. L. Chen, C. Zhou, Y. Cai, L. Ren, and Z. G. Zhang, Laser Phys. Lett. **6**, 657 (2009).
16. A. Chong, J. Buckley, W. Renninger, and F. Wise, Opt. Express **14**, 10095 (2006).
17. J. Fekete, A. Cserteg, and R. Szipoocs, Laser Phys. Lett. **6**, 49 (2009).
18. N. J. Doran and D. Wood, Opt. Lett. **13**, 56 (1988).
19. F. O. Ilday, F. W. Wise, and T. Sosnowski, Opt. Lett. **27**, 1531 (2002).
20. E. A. Kuzin, N. Korneev, J. W. Haus, and B. Ibarra-Escamilla, J. Opt. Soc. Am. B **18**, 919 (2001).
21. O. Pottiez, B. Ibarra-Escamilla, and E. A. Kuzin, Opt. Comm. **281**, 1037 (2008).
22. B. Ibarra-Escamilla, O. Pottiez, E. A. Kuzin, J. W. Haus, R. Grajales-Coutiño, and P. Zaca-Moran, Opt. Comm. **281**, 1226 (2008).
23. G. P. Agrawal, *Nonlinear Fiber Optics* (Academic, San Diego, 1995), Chap. 6.